The International Journal of Advanced Manufacturing Technology (2024) 132:873–892
https://doi.org/10.1007/s00170-024-13414-0

ORIGINAL ARTICLE

The influence of submillimeter morphological variations on the wettability of WEDM-fabricated dual-scale roughness aluminum alloy 6082 surfaces

Dimitrios Skondras-Giousios[1] · Panagiotis Karmiris-Obratański[1,2] · Magdalena Jarosz[3] · Beata Leszczyńska-Madej[4] · Angelos P. Markopoulos[1]

Received: 4 January 2024 / Accepted: 9 March 2024 / Published online: 18 March 2024

Abstract

Deriving inspiration from natural hierarchical superhydrophobic surfaces, multi-scale structures were manufactured on AA6082 surfaces via wire electrical discharge machining (WEDM), featuring microscale texture due to spark erosion, superimposed upon a wide-range simple and more complicated geometries of submillimeter profiles. The effect that the higher-order scale morphologies had on wettability was investigated. The dual-scale morphology elevated the hydrophobicity of the surfaces compared to single-scale or unmodified surfaces, reaching superhydrophobicity (151°) in the case of a certain triangular profile. Rectangular and triangular profiles facilitated the higher contact angles, while re-entrant geometries were able to totally prevent cavity wetting. A correlation of static contact angle with roughness parameters of the larger scale such as Ra, Rz, Rp, Rsk, and Rku for certain geometry configurations was identified. Peak hydrophobicity resulted at Ra = 70 μm, Rz = 240 μm, and Rp = 160 μm concerning simple geometries. Negative Rsk and Rku > 1.5 affected negatively contact angle of samples. All investigated tested types were found to reach higher hydrophobicity at moderate drop volumes (5 μl). The fabricated samples were anisotropic in at least two directions, showing decreased hydrophobicity in the front, parallel to the groove direction. When tested in multi-directional dynamic tilting up to 90°, the more complicated geometries were able to retain resistance to spreading. All samples demonstrated superliquiphilicity with lower surface tension liquids, making them strong candidate in applications such as oil/water separation. Finally, all samples tested sustained their hydrophobic character subsequent to a 3-month atmospheric exposure period.

Keywords Dual-scale features · Morphology · Roughness · WEDM · Hydrophobicity · Anisotropy

1 Introduction

Constantly evolving for millions of years, extraordinary mechanisms and functions of living organisms can offer numerous solutions in various engineering fields. In the field of surface engineering, fabrication of bioinspired surfaces has gained much interest, in the past two decades. Engineering surfaces inspired from the Lotus or rice leaf, as well as butterfly wings, may gain attributes such as hydrophobicity, directional wettability, anti-corrosion, self-cleaning, or drag reduction [1–3]. Such attributes are obtained mainly due to submillimeter hierarchical structures of these surfaces. Lotus leaves possess a dual-scale dimple-like hierarchy that efficiently traps air when wetted, following the Cassie-Baxter regime, leading to superhydrophobicity and corrosion restriction [4, 5]. Rice leaves and butterfly wings possess similar properties, but their grooved structures induce

✉ Panagiotis Karmiris-Obratański
karmiris@agh.edu.pl

1 School of Mechanical Engineering-Laboratory of Manufacturing Technology, National Technical University of Athens, Athens, Greece

2 Advanced Manufacturing Laboratory, Department of Manufacturing Systems, Faculty of Mechanical Engineering and Robotics, AGH University of Krakow, Krakow, Poland

3 Department of Physical Chemistry & Electrochemistry, Faculty of Chemistry, Jagiellonian University, Gronostajowa 2, 30-387 Krakow, Poland

4 Department of Materials Science and Non-Ferrous Metals Engineering, Faculty of Non-Ferrous Metals, AGH University of Krakow, 30-059 Krakow, Poland

directionality in their wetting properties and efficient drag reduction [6].

The fundamental wetting principles that these structures rely on for increasing their hydrophobicity are related to roughness amplitude increase. For a wetted surface near a hydrophobic region, the roughness increase will lead to rise of hydrophobicity according to the Wenzel's model of homogeneous wetting [7]. To obtain contact angles in the superhydrophobic region ($\theta > 150°$) a heterogeneous wetting state must exist, where air entrapment facilitates the further rise of contact angle. This state is described by the Cassie-Baxter wetting model [8], where the apparent contact angle increases with the expansion of the air/liquid fraction of the wetting interface. The superposition of more than one scale of roughness, in a hierarchical arrangement, will lead to increased contact angles and more stable superhydrophobic wetting regimes compared to single-scale roughness surfaces, according to the multi-scale model of wetting, where the before-mentioned wetting models are essentially applied consecutively for every roughness scale [4].

Therefore, one the most crucial design criteria for achieving the desired surface properties, which stem from superhydrophobicity, is the fabrication of multi-scale structures [9]. Numerous manufacturing methods have been applied during the past two decades in realizing such attributes in engineering surfaces. Of particular interest are metallic surfaces due to their wide range of application as well as the often-demanding manufacturing methods that need to be employed. For obtaining small-scale hierarchical grooved features on difficult to process materials such as metals, traditional and advanced manufacturing methods have been proposed. Microchannels combined with one order of magnitude smaller features were created by elliptical vibration cutting on metallic specimens, enhancing the anisotropic wetting of the machined surfaces [10]. Using a common milling machine for creating grooved microstructures on aluminum combined with stearic acid surface modification, superhydrophobic surfaces with corrosion resistance were created [11]. Major pillars with microgrooves were manufactured on brass-360 alloy surfaces by DTM (diamond turning machining) process, improving the hydrophobicity of the prepared surfaces [12]. Combining mechanical surface broaching and chemical oxidation, a double-scale superhydrophobic copper surface was created, with anisotropy on dropwise condensation [13]. Implementing a 2D compliant vibration-assisted cutting method, a hierarchical surface on aluminum 6061 was created, exhibiting higher hydrophobicity compared to the smooth surface [14]. A hierarchical structure of diamond-cut microgrooves, along with rectangular-shaped cuprous oxide produced from hydrothermal synthesis [15], shows hydrophobicity and corrosion resistance. By combining sintering and grafting, superhydrophobic Cu with hierarchical porosity was fabricated [16]. By tuning the annealing states and controlling the extend of bending, different hierarchies on fracture metallic glasses surfaces were fabricated, exhibiting different wetting properties [17].

Thermal-based methods are often used for fabricating hierarchical grooved structures on metallic materials. Laser fabrication offers the advantage of creating microstructures by precisely ablating the material, while the remelting of expelled material simultaneously creates nanostructures. By adequately tuning the focal position and period during femtosecond laser ablation, superhydrophobic microridges with superimposed submicron convex feature were created on stainless steel surfaces [18]. Femtosecond laser fabrication was also used for fabricating ordered microstructures combined with smaller structures created from nanosized laser-induced periodic surface structures (LIPSS) on stainless steel surfaces, inducing hydrophobicity [19]. Superior anti-icing properties of micro-nano-textured aluminum alloy surface with various groove sizes were constructed by picosecond laser ablation [20]. Using underwater multipass nanosecond laser treatment on aluminum workpieces, anisotropic hierarchical grooves of different heights were created, exhibiting hydrophobic properties and efficient dynamic water manipulation [21].

Another thermal based process that has been proved to be very effective on inducing hydrophobicity on metallic surfaces is wire electrical discharge machining (WEDM). Dual-scale surface structures can be created by the principle of WEDM operation. Through a one-step process, larger features can be produced by programming the electrode tool path, while smaller random crater features are created simultaneously by material removal due to material ablation from plasma microchannels, ultimately constituting the needed hierarchy that can induce hydrophobicity on surfaces of various conductive materials [22–24]. V-shaped grooves on stainless steel surfaces were created with high-speed WEDM technology, retaining their hydrophobicity after wear test of 0.5 m sliding distance [25]. Various depths of grooves made by WEDM were compared in terms of controlling water and oil wettability [26]. Various re-entrant geometries fabricated by WEDM on steel surfaces were tested for wettability, where mushroom-shaped, narrow structures with wide spacing were found to be preferable for water repellence [27]. The deepest groove of 200 μm was found to be more effective for oil/water separation. A combination of WEDM and a solution immersion method was used to fabricate three-level hierarchical structure of 5083 Al alloy surfaces, gaining amphiphobic properties to water, glycerol, and ethylene glycol [28]. Inspired by the natural superhydrophobic surfaces of lotus leaf and cicada wing, array microstructures of various dimensions on 7075 aluminum surface were created [29]. The height was proved to be the most crucial factor for increasing contact angle and reducing contact time. Smaller than conventional WEDM microgroove surface was

produced by low-frequency vibration assistance, improving the hydrophobic properties of copper surfaces [30]. Hierarchically grooved copper surfaces prepared by WEDM showed superior condensation heat transfer performance compared to flat hydrophobic copper plates, showing structure property relationship [31]. The effect of various submillimeter sinus and rectangle morphologies on hydrophobicity was studied on a Cu-alloy surface prepared by WEDM, finding optimal periods for obtaining greater hydrophobicity [32]. The hierarchical structure of Ti6Al4V surface prepared by WEDM has proved to exhibit better anti-bacterial properties compared to the unstructured surface, strongly related to the decrease of surface energy [33]. Hierarchical grooved structures prepared by WEDM on aluminum were tested for hydrophobicity after few days of exposure and were found to dramatically increase their apparent water contact angle due to absorption of organic elements [34]. A superhydrophobic copper mesh for oil/water separation and fog collection was created by combination of WEDM and low surface energy modification. Controlling the wire path, various combinations of surface structures could be created [35]. Finally, a comparative study on copper and brass surfaces with WEDMed microcolumns and microstrips showed the influence of droplet size as well as the material and structure dependency on static and dynamic wettability [36].

In addition to the above-mentioned experimental studies, some research has been reported for modeling or theoretical aspects of the wettability analysis for two-scale hierarchical structures, similar to those manufactured by WEDM. Modeling a two-scale hierarchy and numerically calculating the droplet profile, it was found that the increase of structure spacing and the decrease of structure height, within certain range, could increase the contact angle and decrease the contact angle hysteresis of the droplet [37]. A mathematical model based on force balance was proposed for the prediction of contact angles of droplets on three different morphology profiles prepared by WEDM and treated with stearic acid [38]. The experimentally validated results showed that the array pillars with semicircular profile showed the better superhydrophobicity. A modeling, based also on force balance, was implemented for predicting the contact angle of different structure profiles prepared by WEDM on gray cast iron, taking into account a simplified profile of the microroughness due to spark erosion [39]. The results showed that better hydrophobic properties were obtained with structures of square column profile.

Although several works examined the wettability of some basic dual-scale geometrical profiles, no study has systematically studied a wide range of profile types on different wettability aspects. In this work, dual-scale surface structures of various profile geometries were manufactured via the WEDM process. The aim was the investigation of the effect that different profile geometries, which act as a higher-order scale morphology, may have on various wettability features. To test this hypothesis, various roughness parameters were measured and compared with contact angle measurements, in order to examine whether there is an independence of geometry correlation of contact angle with roughness. Other geometrical effects on contact angle, such as anisotropy on two or three directions during surface tilting, were tested. The effect of different droplet volumes was also taken into account on contact angle measurements. In addition, lower surface tension liquids and various liquid volumes were also tested in order to enhance the produced results and the knowledge on the studied effects.

2 Materials and methods

2.1 Materials

In the research, an AA6082 aluminum alloy in a T6 temper state was employed. This particular metal alloy is categorized within the 6xxx series of aluminum alloys, which are systematically identified as precipitation-hardenable alloys. The T6 temper signifies a specific method of heat treatment that optimizes the material's characteristics, making it highly suitable for a variety of applications. This series of aluminum alloys is renowned for its ability to be strengthened through precipitation hardening, a process that significantly improves its mechanical properties. It fundamentally comprises aluminum, while magnesium (Mg) and silicon (Si) function as the pivotal alloying constituents. The conventional chemical makeup of AA6082 is delineated as fluctuating between 0.7 and 1.3% Mg and 0.4 and 1.0% Si [40]. The alloy samples, in T6 temper, underwent a thorough heat treatment process involving solution heating at 530 °C for 8 h, quenching, and subsequent artificial aging at 180 °C for 8 h to induce the precipitation of Mg_2Si phases [41, 42]. Owing to its propitious strength-to-weight ratio, AA6082 is extensively utilized in structurally critical components across aerospace, automotive, and marine engineering domains [43]. This specific alloy manifests a tensile strength approaching 330 MPa, a yield strength that spans between 100 and 290 MPa, and hardness oscillating within the 80-HV range. Subsequent Table 1 elucidates the detailed chemical constitution of AA6082.

2.2 Methods

2.2.1 Fabrication method—wire electric discharge machining (WEDM)

The surfaces were machined utilizing a WEDM (Neospark B500, Knuth Germany) and employing a molybdenum wire. First, the aluminum samples were affixed to the WEDM and

Table 1 Chemical composition of AA 6082

Al	Mg	Mn	Fe	Si	Cu	Zn	Cr	Ti
Bal	0.9	0.7	0.5	1.0	0.1	0.1	0.2	0.11

then cut to ensure the flatness of each sample. The dimensions of the AA6082 samples were 15 × 40 mm. After a certain number of test runs, the machining process was monitored, using constant machining conditions of pulse-on currents (Ip) of 2A, pulse-on time (Ton) of 20 µs, and pulse-off time (Toff) of 90 µs, to reduce electrode wear and enhance the surface quality of the process. It is important to note that surface roughness corresponding to the specific machining parameters is constant and in the order of few microns and differs from the measured roughness of the dual-scale structures presented in the next sections, which refers to a submillimeter scale of hundreds of microns. The dielectric fluid that was used during machining was deionized water. After processing, the samples were cut to a thickness of 5 mm. An illustration of the overall manufacturing procedure can be seen on Fig. 1.

2.2.2 Contact angle (CA) measurements

Before the CA measurements, the samples were cleaned in the ultrasound bath in ethanol, acetone, and water for 5 min each. All CA measurements were performed using an OCA25 goniometer with a TBA100 holding system (DataPhysics), equipped with an automatic dosing system and SCA20 software at an ambient temperature. Deionized water was used for CA measurements of all of the samples. Depending on the measurements, different dosing volumes were applied (i.e., 2, 5, and 10 µl) with a constant dosing rate of 0.2 µl·s^{-1}. Before photographing the deposited droplet, the waiting time was set to 30 s to prevent any dynamic effects. The total number of 3–5 droplets on each sample was deposited and measured. The droplets were deposited at samples from two directions—front and side for the morphology-related measurements. For the selected samples, the time-dependent CA was measured. Therefore, the measurements were repeated after 90 days using the same protocol.

The values of CA were measured using SCA20 software, where a contour analysis was performed. For selected samples, the dynamic contact angle was measured using the tilting method. Samples were mounted on the table, and the droplet of 2 µl was put on the surface. The tilting procedure was established in the software. The table was gradually tilted from 0 to 90°, and a movie was recorded. Depending on the morphology, measurements were performed either bi- or tridirectionally. The CA values were determined automatically using SCA20 software. The automatic mode was not useful for some samples, so the manual contour analysis was applied.

2.2.3 Surface roughness, topography, and chemical composition evaluation

An investigation into the surface topography (ST) was performed by using three different methods. Due to the dual-scale roughness nature of the specimens, the surface roughness (SR) needs to be analyzed macroscopically by defining the surface texture and microscopically by defining the SR.

At first, the surface texture parameters were analyzed using a focus variation microscope (FVM) to verify the macroscopic surface topography and its characteristics [44]. A VHX-7000 ultra-deep-field microscope (KEYENCE, Mechelen, Belgium), equipped with a × 20–2000 objective was utilized. This technique is similar to confocal microscopy, and the measuring method of an FV microscope is based on a white light LED source that passes through a semitransparent mirror and a lens before it reaches the measuring surface. Then, the reflected light from the focused areas returns through the lens, and a beam splitter directs it onto a photonic detector, which registers the geometric and photometric information [45]. In other words, FV can deliver colorful, high-resolution 3D surface measurements

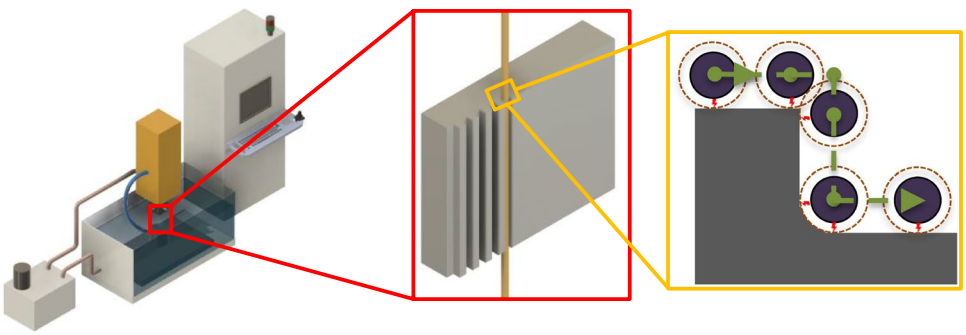

Fig. 1 Schematic of the WEDM process

by merging the small depth of a classical optical system and vertical scanning.

In the determination of the secondary, smaller scale roughness, a TOPO 01P contact profilometer was utilized, endowed with an induction measuring head, and further characterized by a diamond tip, exhibiting a cone morphology with a 2-µm radius and a 90° apex angle. The investigative apparatus was structured with a confocal sensor, substantiated by a 130-µm range and an 8-nm vertical resolution. Employing a Gaussian filter, predicated upon Fourier transformation, specific cut-off lengths were delineated. This metric concomitantly dictated which components of the measured profile—or intrinsic surface components—would be assimilated as quantifiable surface roughness, while concurrently suppressing others. SR analyses were conducted on an arbitrarily selected machined surface, in stringent adherence to established norms, utilizing a cut-off of 2.5 ls and a stipulated evaluation length of 2.5 mm. The flat samples machined by the same conditions were measured 30 times [46] and the average microscale roughness parameters were found to be Ra = 3.2 µm, Rz = 15.7 µm, Rsk = 0.11, Rp = 8.62 µm, Rv = 7.13 µm, and Rku = 2.48.

Finally, the microscopic and chemical analysis involved a Hitachi SU 70 scanning electron microscope supplemented with EDS analysis. During the utilization of the secondary electron (SE) or backscattered electron (BSE) detector, microphotographs were captured, operating at accelerating voltages of 10 and 15 kV. EDS analysis facilitated the pinpointing and mapping of chemical elements within designated microareas, furnishing critical insights into compositional fluctuations of the machined surface.

3 Results and discussion

3.1 Double-scale surface texture characterization

Double-scale surface profile textures of circular, triangular, rectangular, mixed rectangular, double-size rectangular, and re-entrant profiles were manufactured. The smaller scale, crater-like roughness on the surface is created due to the plasma discharges during machining and covers the whole surface. The micromorphology can be seen in the SEM images of Fig. 2 for up to × 1000 magnification for a rectangular shaped profile. It can be clearly seen from Fig. 2d and e that the surface is covered with discharge pits and protrusions that induce roughness, as compared to a flat surface and can facilitate the anti-wetting attribute. Microcavities can resist wetting by entrapping air inside them leading to a composite Cassie-Baxter regime [47]. The WEDMed microroughness can alter according to machining parameters such as pulse-on time T_{on} and maximum current between electrodes I_p and servo voltage SV and consequently can affect the wettability of the surface [48]. Given that the experimental objective was to identify the effect of different profile morphologies, the discharge parameters were kept constant in order for the microroughness to be the same for all the profiles.

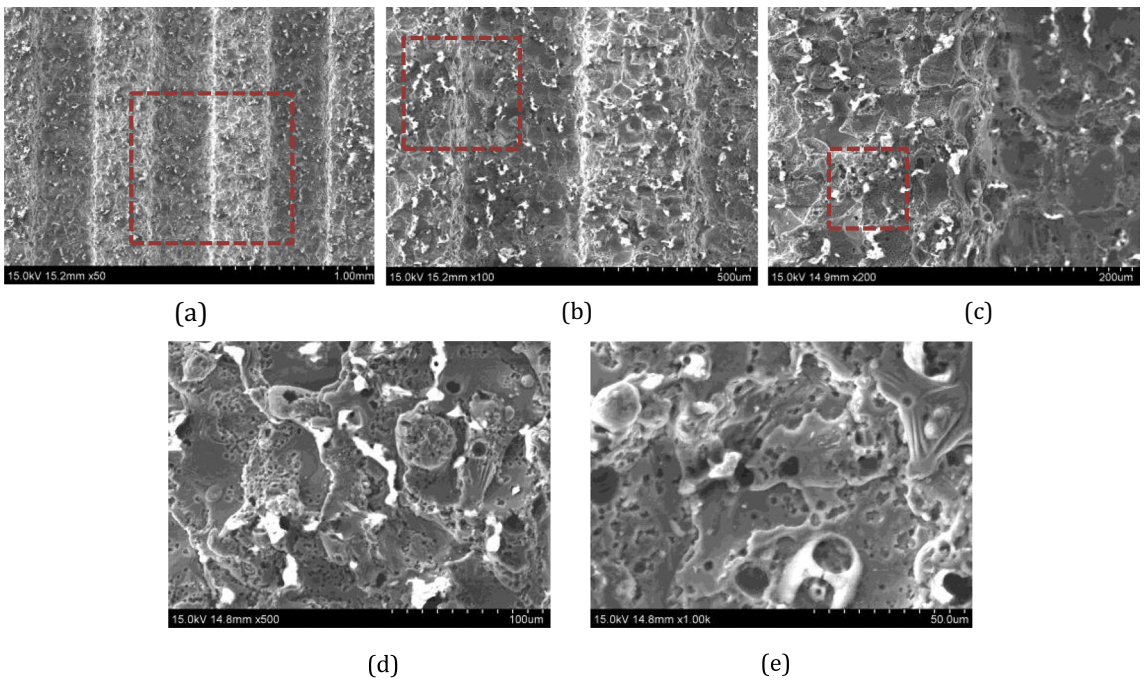

Fig. 2 SEM images of the machined surface of rectangular shaped geometry profile: **a** × 50, **b** × 100, **c** × 200, **d** × 500, and **e** × 1000

A crucial component of wettability lies on the chemical composition of the examined surface due to its influence on surface energy. It is important to identify possible changes in the chemical composition of the surface after electrical discharge machining. As the discharges occur, part of the material of the electrode wire might be permanently transferred to the specimen's surface and slightly modify the final composition. The wire material that was used for the surface modification of the specimens was molybdenum. The EDS and EDAX analysis of the modified surface of the aluminum alloy indeed revealed traces of molybdenum, as Fig. 3 shows. However, molybdenum is not reported to decrease the surface energy. A component of the rise of hydrophobicity can be partially attributed to the presence of C in the surface. Increased carbon content has been reported as a factor that contributes to the wettability transition of aluminum surfaces after being machined by thermal processes such as EDM [34, 49] or laser machining [50, 51]. Oxygen is also present, which might be a cause of increase in the final surface energy of the specimens.

Superimposed to that microtexture, profiles with different geometries were manufactured from the CNC path of the wire. The final geometries were slightly different than the designed ones due to a bilateral wire cutting offset of 25 μm, measured by the extra width added to the wire diameter on the width of a single machined groove. Morphologies of different geometries as well as different submillimeter dimensions were fabricated. Basic geometries of groove profiles such as circular, triangular, and rectangular were fabricated with different lengths and depths. These geometries can cover a satisfying range of different curvatures that droplets will be in contact with. In Fig. 4a–c, three basic geometries of circular-, triangular-, and rectangular-shaped protrusions with their profiles and 3D microscope images can be seen. Apart from the basic groove geometries, more complex groove geometries were manufactured in order to investigate possible effects of the induced complexity on the wettability of the surfaces. Such geometries can be seen in Fig. 5. A profile with two different groove dimensions can be seen in Fig. 5a, a step-like groove profile can be seen in

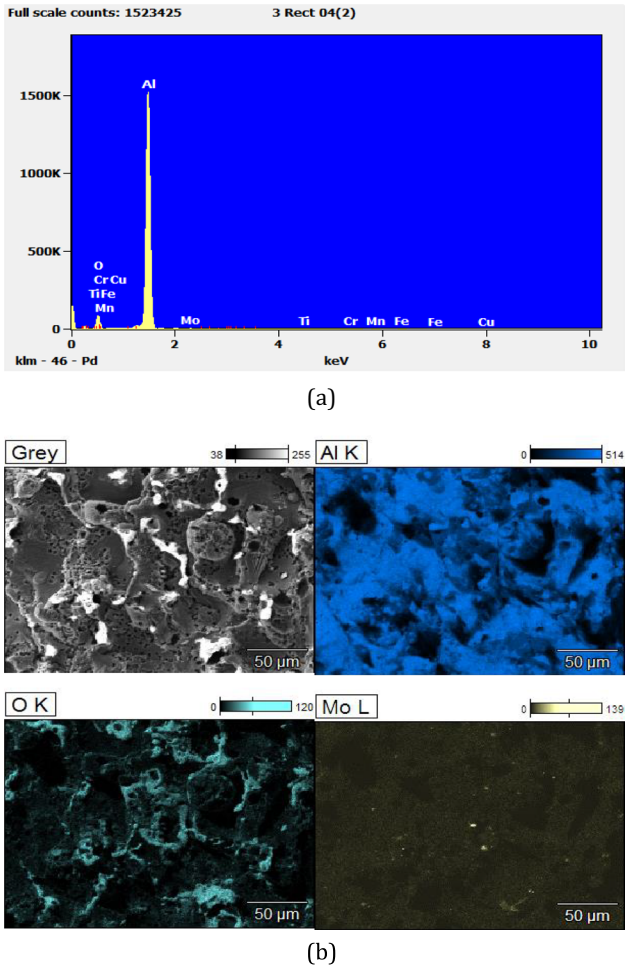

Fig. 3 EDS (**a**) and EDAX (**b**) of the surface after WEDM process

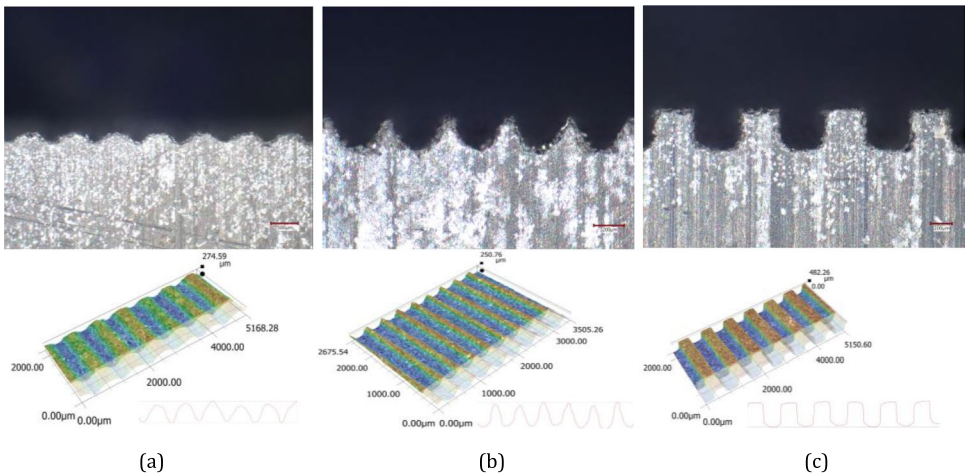

Fig. 4 Manufactured groove profiles of basic geometries: (**a**) circular, (**b**) triangular, and (**c**) rectangular

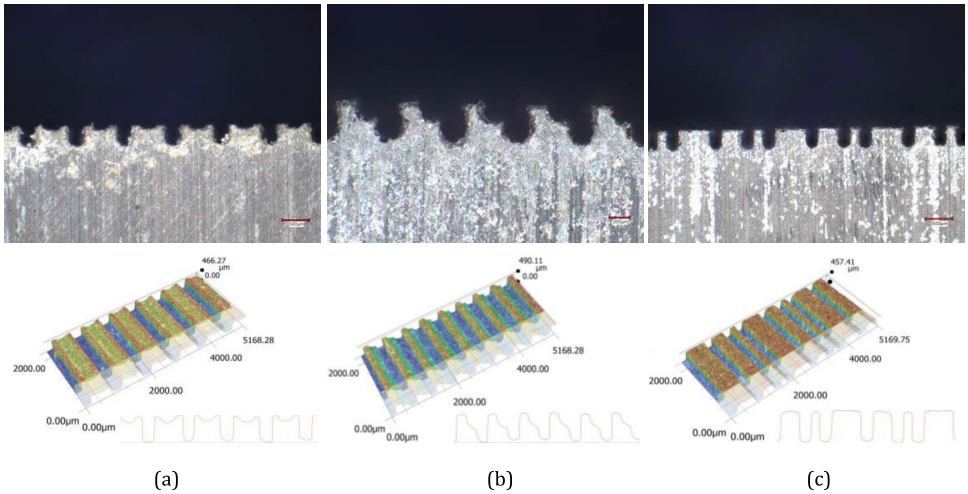

(a) (b) (c)

Fig. 5 Manufactured groove profiles of complex geometries: (**a**) double rectangular, (**b**) step-like, and (**c**) altering width

Table 2 Contact angles of three aluminum samples with different scales of roughness

	Flat	Single-scale microroughness	Dual-scale roughness
Contact angle	66° ± 7°	103° ± 6°	137.52° ± 2°

Fig. 5b, and an altering protrusion width pattern can be seen in Fig. 5c.

The single-scale microroughness of the eroded samples, without geometrical features combined with the chemical enhancement of C, O, and Mo due to the discharge process, improved their hydrophobic behavior, raising their water CA to 103.61°, compared to the 66.15° of the flat, non-eroded sample. This surface modification towards hydrophobicity from straight WEDM cut on aluminum alloys surfaces has already been reported [22]. The introduction of geometrical features on the aluminum samples, creating a dual-scale morphology, led to an additional rise on their hydrophobicity for almost all cases considered, as will be thoroughly discussed in Sect. 3.2. In Table 2, the contact angles of a flat, a single-scale eroded and the dual-scale eroded sample of Fig. 4c can be seen. This is a one-step method, without the use of any extra surface treatment.

3.2 The effect of different morphological features and second-scale roughness parameters on wettability

In this section, the effect that different geometrical profile patterns can have on the final wettability of the surface is explored. In Table 3, the produced geometrical shapes along with their measured submillimeter dimensions are reported. Their respective contact angles for 5-µl drop volume are depicted as well in Fig. 6. The categorization of the groups is based on their morphology complexity. Basic geometrical shapes of circular, triangular, and rectangular profiles are denoted with C, T, and R. More complex geometrical shapes of double-sized grooves, mixed protrusion widths, and re-entrant profiles are denoted with D, M, and I. The manufactured lengths varied from 230 up to 800 µm and the depths varied from 60 up to 600 µm. The lower dimension limit of the length can be attributed to the width of the wire, while for the upper dimension, limit of both length and depth of the features arises from the maximum volume of the droplet that was used, so that the groove dimensions are comparable with the maximum droplet diameter.

It can be observed that for all cases, except D2, all the dual-scale morphology samples show static contact angles (SCA) significantly higher compared to the single-scale morphology presented in Table 1, for 5-µl droplet volume. The rise of SCA, when a second scale of roughness is introduced to the surface, is mainly attributed to the hierarchy of the surface morphology, when the surface is not intrinsically hydrophilic [52]. The mean rise of the SCA from all the samples compared to the single-scale roughness was nearly 30°. From the manufactured profiles, the rectangular geometry profile had the highest mean SCA (141.5°), while the double geometries had the lowest mean SCA. In Fig. 6, it can be clearly observed that profile geometry seems to play a crucial role on the SCA. While all the produced samples possess the same microroughness, the effect of the second-scale features can alter the SCA from 90° in the D2 case up to 151° in the case of T4. Sharper geometries like T and R can hold the triple line of the liquid more conformed than smoother geometries such as C. Moreover, a difference in wetting states was observed throughout different groups of the profile features. Wenzel-state hydrophobicity was exclusively observed in the C, T, and D groups. A mixed state of Wenzel and Cassie-Baxter regime was observed in R and D groups, preventing some cavities from wetting. A

Table 3 Geometry types, dimensions, and mean contact angles of the samples (C, circular; T, triangular; R, rectangular; M, mixed length; I, re-entrant; D, double)

Geometry		L (μm)	D (μm)	Ca(°)
C	1	400	60	114±0.5
	2	600	125	132±5
	3	800	200	134±5
T	1	200	60	107±7
	2	400	120	140±7
	3	400	200	148±5
	4	400	250	153±2
R	1	250	200	140±1
	2	350	300	150±8
	3	380	350	143±4
	4	420	400	133±2
M	1	230	200	143±5
	2	230	400	136±7
	3	230	600	116±5
I	1	230	400	131±3
	2	230	380	140±4

D		L_1	L_2	D_1	D_2	
	1	330	280	200	300	140±8
	2	300	200	85	365	90±3
	3	350	400	175	385	137±1
	4	280	300	90	380	118±5
	5	410	220	195	375	137±2

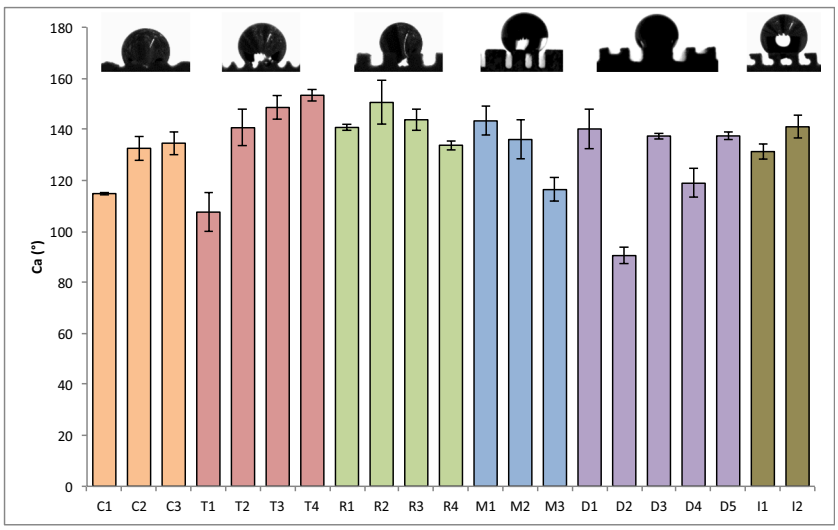

Fig. 6 Contact angles for all manufactured geometries

pure Cassie-Baxter state was observed in the case of the I group, where no cavity was wetted. Re-entrant geometries can facilitate the Cassie-Baxter state [53].

In the relevant literature, trends of contact angles with altering dimensions have been reported, having mixed results. In this study, the increase of depth was found to increase the contact angle of T profiles up to depth of 250 μm tested. This result is in agreement with studies on triangular profiles at similar widths and depths [26, 54, 55]. A similar increasing contact angle trend with increasing height and depths was observed for the C group. In the R group, the increasing size of features was found to increase the contact angle up to 300-μm depth for the R2, followed by a small decrease for increasing feature size up to R4. Therefore, a size limit was reached regarding wettability, after which an important portion of droplet volume is located within the cavities. The M group was designed with the periodicity in altering length sizes of the features, with depth of grooves increasing from M1 to M3. Despite the altering length of the features, depth variation resulted to dictate the contact angle evolution, by decreasing it with increased depths up to 600 μm. The D group showed more uneven wettability results. The inclusion of dual profiles consisting of larger and smaller grooves reduced the contact angle in the D2 and D4 profiles which were designed with significantly smaller groove depths, for the smaller sized grooves. The smaller groove depth increase from 85 up to 200 μm resulted in monotonically increased contact angle from 90 up to 140 μm. The re-entrant profile group I resulted in different contact angles, although the height and length values were very close. However, I1 had a larger groove area and spacing, which could induce the droplet to spread more on the surface than I1. The D5 and I2 types are complementary with each other. The repeated feature of D5 (Fig. 5b) is the repeated groove of I2 (top right image of Fig. 6) and vice versa. Although I2 can effectively trap air inside the groove and D5 does not, their difference in contact angle is only 3°. This indicates that the air entrapment at the mesoscale does not have a significant effect on the apparent contact angle. However, a Cassie-Baxter-like regime can be advantageous in applications where the complete non-wetting of the grooves could be important such as anti-icing or self-cleaning.

The dimensions and spacing of the features are important in cases that a specific type of feature is studied. Keeping the other dimensions constant and for selected profile types, depths over 150 μm have been found to decrease contact angle in dual-scaled textures produced by WEDM [25, 28]. Spacing and width of features have been found less important than depth in contact angle manipulation [29] [35]. Comparisons between different profiles of same dimensions and spacing resulted in differences in the wettability of the various profiles [32, 38, 39]. The possible combinations of sizes and shapes of the features are a very large number; thus, the wettability outcome is difficult to predict and should be considered for each individual case. For that reason, a more universal approach for the characterization of the influence of the submillimeter morphology on hydrophobicity was employed in this work, by measuring the mesoscale roughness of the textured surfaces. Therefore, the examination of wettability variation of the mesoscale structures was examined under the prism of their mesoscale roughness. The obtained roughness parameters for all samples are presented in Table 4. The roughness parameters were measured for the second scale of roughness, meaning that effects of the microroughness, which is the same for all samples due to the same machining parameters used in each case, were not taken into account. The purpose for that was to explore solely possible effects of the larger scale features of the surfaces.

The roughness amplitude parameters Ra, Rz, and Rp of all profiles were measured and compared with SCA measurements, in order to investigate the effect of peak-to-valley amplitude on wettability. Textures with dual-sized grooves (D1–D4) may introduce mixed results on wettability as seen above, due to the effect of the smaller groove depth. Considering the textures with single-sized grooves, the plots of the contact angles with roughness parameters Ra and Rz are seen in Fig. 7. Contact angle values exhibit an increasing trend with a following decrease after reaching approximately 100 μm and 300 μm for Ra and Rz respectively. Figures 5, 6, and 7 are indicating that textures with different dimensions follow a general trend that is related with roughness amplitude. Roughness amplitude increase is beneficial for lowering wettability until a threshold. After reaching that threshold, wettability is increased again. Re-entrant (I1 and I2) and mixed length (M1–M3) might induce a slightly distorting effect on some aspects of wettability. I and M geometry groups are actually not fully wetted in all cases, while the M group has length variations induced that might induce variations in spatial frequencies.

Concerning the basic profile geometries C, T, and R, a 2rd-order polynomial correlation was found, with SCA and Ra, Rz, and Rp, with $R^2 > 90\%$ for all three roughness parameters, as Fig. 8 shows. These results imply that those roughness parameters have a stronger influence on SCA compared to the different geometries of the sample profiles. Although the fabrication of profiles serving as a second scale of roughness indeed was found to increase the SCA, it seems that the geometry type does not affect significantly the SCA. The SCA trend was found to be the same for all three parameters, showing an increase of SCA with the roughness increase until a critical point, after which the decrease of SCA with increasing roughness is observed. The highest SCA was found at moderate values of Ra = 70 μm, Rz = 240 μm, and Rp = 160 μm, while for higher or lower values of those roughness parameters, the SCA was lower.

Table 4 Roughness parameters of the textured profiles

	Ra (μm)	Rz (μm)	Rp (μm)	Rv (μm)	Rsk	Rku
C1	16.35	74	36	38.06	−0.08	1.83
C2	34.31	140.48	62.33	78.15	−0.25	1.84
C3	47.44	171.59	74.38	97.21	−0.34	1.68
T1	9.74	81.5	32.83	48.46	0.18	3.37
T2	37.44	139.28	78.81	60.47	0.39	1.69
T3	58.21	211.68	121.1	90.6	0.52	1.75
T4	75.83	246.92	160.3	86.62	0.67	1.79
R1	58.91	172.92	88.46	84.46	0.03	1.28
R2	114.84	284.51	141.12	143.38	0.04	1.13
R3	139.1	385.35	168.2	217.12	−0.29	1.16
R4	173.15	417.22	218.86	198.37	0.09	1.01
M1	62.31	183.82	68.15	115.67	−0.58	1.56
M2	148.1	386.44	138.64	247.8	−0.56	1.44
M3	240.21	611.46	214.03	397.43	−0.69	1.53
D1	98.59	316.67	132.6	184.07	−0.077	1.44
D2	105.73	417.19	128.27	288.2	−1.31	3.01
D3	129.01	418.38	183.79	234.59	−0.35	1.56
D4	132.9	409.59	157.8	251.79	−0.7	1.7
D5	122.27	384,77	195.72	189.05	−0.04	1.49
I1	121.92	405.6	189.1	216.5	−0.143	1,56
I2	114.28	392.9	190.5	202.4	−0.045	1.61

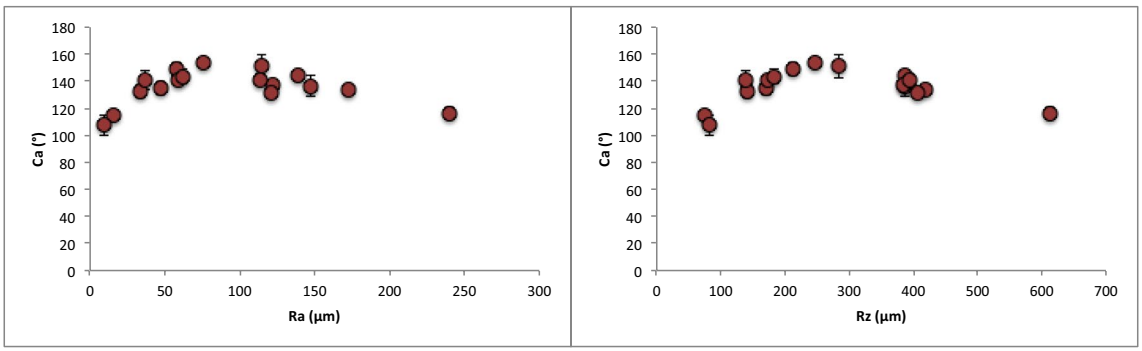

Fig. 7 Plots of contact angle value evolution with Ra (left) and Rz (right) for all the samples except the dual-scaled grooved types (D1–D4)

The increasing SCA with the increase of Ra for values up to 80 μm is also reported in EDM machined surfaces [48]. Interestingly, the same trend was not observed with Rv, posing an indication that profile peaks might have a stronger correlation with SCA. The same roughness values of more complex geometrical profile groups of D, M, and I were not found to have any particular correlation with SCA values. More specifically, as noticed above, the complex geometries seem to induce a negative effect on SCA for Ra values adjacent to the simple ones. Thus, hydrophobicity is not favored from geometric complexity of the profiles.

Additionally, the higher order roughness parameters of skewness Rsk and kurtosis Rku were also measured for the second scale of roughness in order to investigate possible effects of profile height distribution on the wettability of the surfaces. Positive values of Rsk indicate the predominance of peaks, while negative values of Rsk indicate the predominance of valleys. Rku denotes how sharp is the profile of a surface, with values over 3 indicating a spiky profile. A map including skewness and kurtosis values of all the samples is depicted in Fig. 9. Considering all morphologies, it is observed that positive and near-zero values of skewness are more favorable for anti-wetting properties of a surface. Gaussian roughness profiles are reported to be favorable for hydrophobicity [56]. This is a second indication of peaks being more crucial than valleys in reducing wettability of the sample surfaces. In addition, increased kurtosis near the "spike" limit has a negative effect on the hydrophobicity of

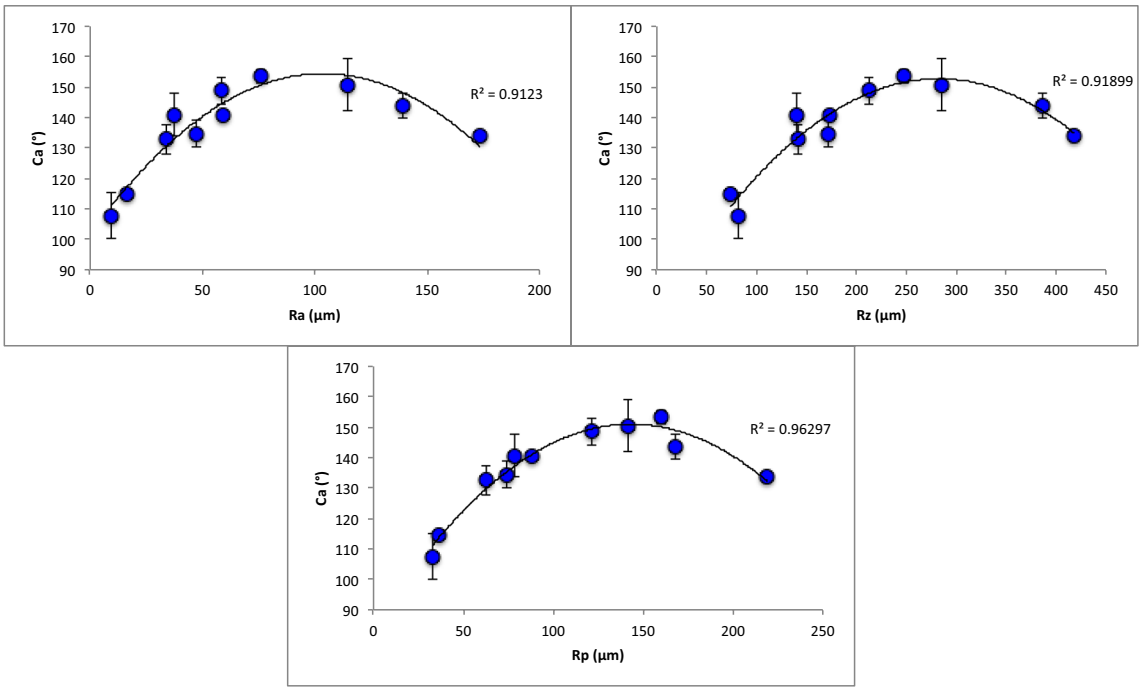

Fig. 8 Contact angle evolution with Ra (top left) Rz (top right) and Rp (bottom) of the C, T, and R groups

Fig. 9 Map of Rsk and Rku roughness values for all profile morphologies

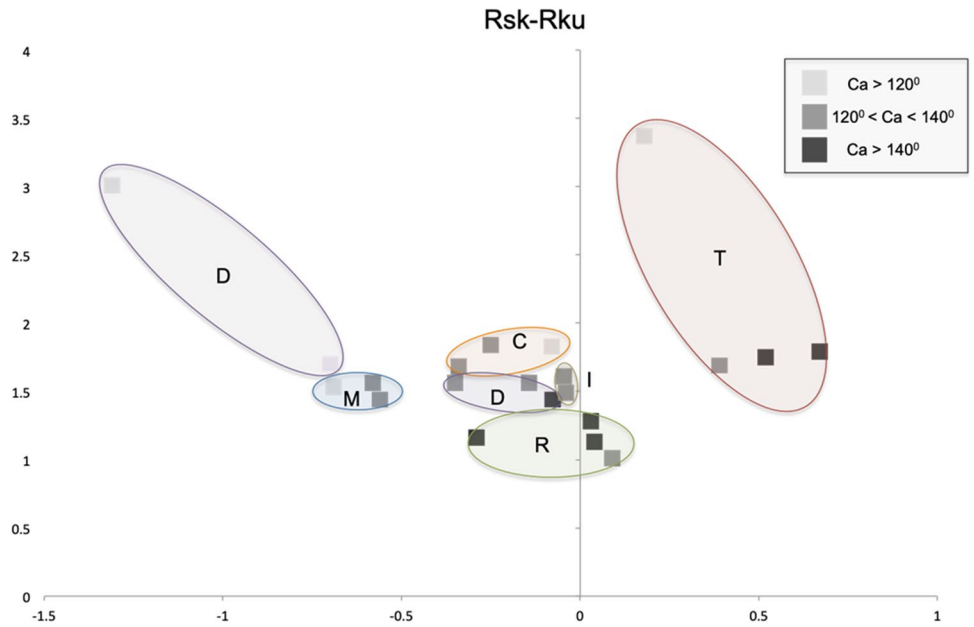

the surface, as can be seen from the higher Rku values of D and T groups. Decreasing values of negative skewness Rsk (< -1.3) combined with increasing values of kurtosis Rku (> 1.6) were found to decrease the hydrophobicity of the surfaces, as noticed in groups D and M. These observations may elucidate the SCA differences found between basic and complex geometry profile groups with adjacent Ra in Fig. 6.

3.3 The effect of profile morphology on multi-directional dynamic wettability

Topographical directionality along one or more directions is assisting the control of wettability features of a surface. Creating anisotropic surface structures, the droplet manipulation becomes possible in a passive but

controllable manner [57, 58]. In this work, all manufactured surface profiles possess directionality in at least one direction. All SCA of samples from the front of the profiles were measured significantly lower than from the side. This difference is attributed to the fact that droplet is not conformed along the direction of the grooves; thus, the droplet spreads more in that direction. However, it is crucial to explore the wetting changes during dynamic conditions. To do so, the tilting of the droplet platform was performed from 0 until 90° in three different directions, as depicted in Fig. 10. In all cases considered, droplets were strongly adhered on the surface and no rolling occurred even after 90° of tilting. However differences between different geometry types were noticed. In this section, simple (C, R, T) as well as complex geometries (D, I) were selected.

For the bidirectional measurements, four profiles of four different groups were selected, C3, R3, D3, and T3. In the bidirectional cases, the contact angle was measured for the tilting directions of the front and the side parts of the samples. In Figs. 11 and 12, the evolution of CA with the tilting angle of the samples can be seen for the selected profiles. The tilting affects the advancing Θ_{adv} and receding Θ_{rec} fronts of the droplet as well as the static contact angle hysteresis (SCAH), Θ_{adv}–Θ_{rec}. In all cases, Θ_{adv} and Θ_{rec} decreased in both front and side directions, indicating a partial soaking of the droplet inside the grooves of the sample surfaces. Concerning the side tilting direction, the lowest decrease in contact angle occurred in the case of C3 with 12°, while the highest decrease was reported in the case of T3 with 45°. Concerning the front tilting direction, the lowest decrease was found in the D4 case with 10°, while the highest decrease was found again in the T3 case with 20°. The only case when an increase was noticed was the D3 geometry type, for the front tilting direction.

Furthermore, the SCAH was measured throughout the different geometry types tested. SCAH can be interpreted as a measure of how strong is the adhesion of the surface and the droplet [59]. In the case of SCAH, the measurements represent the Θ_{adv}–Θ_{rec} in the highest tilting angle of 90°. It can be observed that the SCAH from the side tilting direction were all found to be under 4° without any significant differences. However, concerning the front direction, the SCAH was found considerably different between different profile types. The lowest SCAH was found in the case of R3 with 2°, while the highest SCAH was found in the T3 type with 13°. The results from the bidirectional tilting of the four different profile types indicate that the anisotropy induced by the grooves does affect the wetting direction that is realized through the partial soaking of the droplets and is parallel to the direction of the grooves. The geometrical shape of the profile had an effect in both side and front tilting directions by either enhancing or weakening the adhesion of the droplet. As tilt angle was increasing, the triangular-shaped T acted as a spreading facilitator in the parallel to the groove direction, while the double-grooved profile D was able to conform more to the spreading of the droplet. The rounded profile C also was able to conform to the droplet spreading. The sharp edges of the T-shaped profile are more likely to guide the droplet in the parallel, and not the perpendicular direction, as the lowest SCAH was found in that profile. In addition, the smaller rectangular-shaped grooves of the double-grooved geometry D are assisting the movement restriction of the droplet in the parallel to the groove direction.

The complex geometrical profiles of D5 and I2 were designed for possessing anisotropy in three directions: front and ± side. These two profiles are actually negative one to another. The maximum contact angle drops when tilt angle was 90° was 27° for the (+) tilting side of the I2 type while the minimum contact angle drops when tilt angle was 90° was 8° for the (+) tilting side of the D5 type, as Fig. 13 shows. In all three directions, D5 type had lower contact angle drop as tilting angle was increasing, indicating lower spreading tendency compared to all measured samples. The SCAH of all the directions for the two types was under 5°, except from the (−) tilting side of I2, which was measured 21°. As can be seen from the inspection of the anisotropy directions of the side profiles, this is the only profile with clear side directionality. Although D5 type has also an anisotropic profile, however, a difference between (+) and (−) tilting side directions in spreading or SCAH

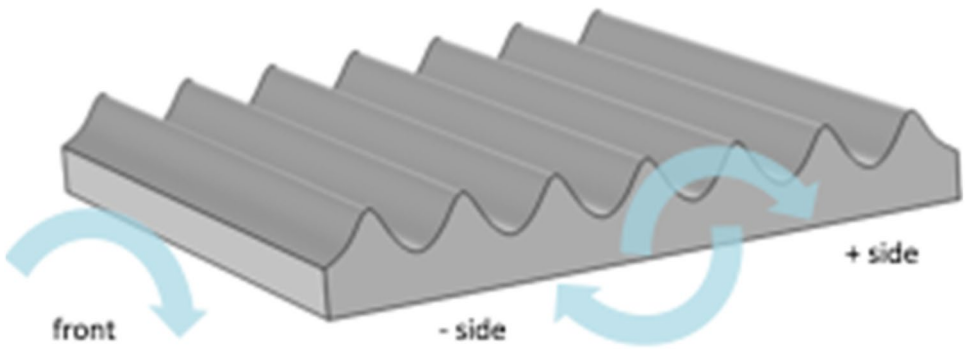

Fig. 10 Tilting directions of the platform

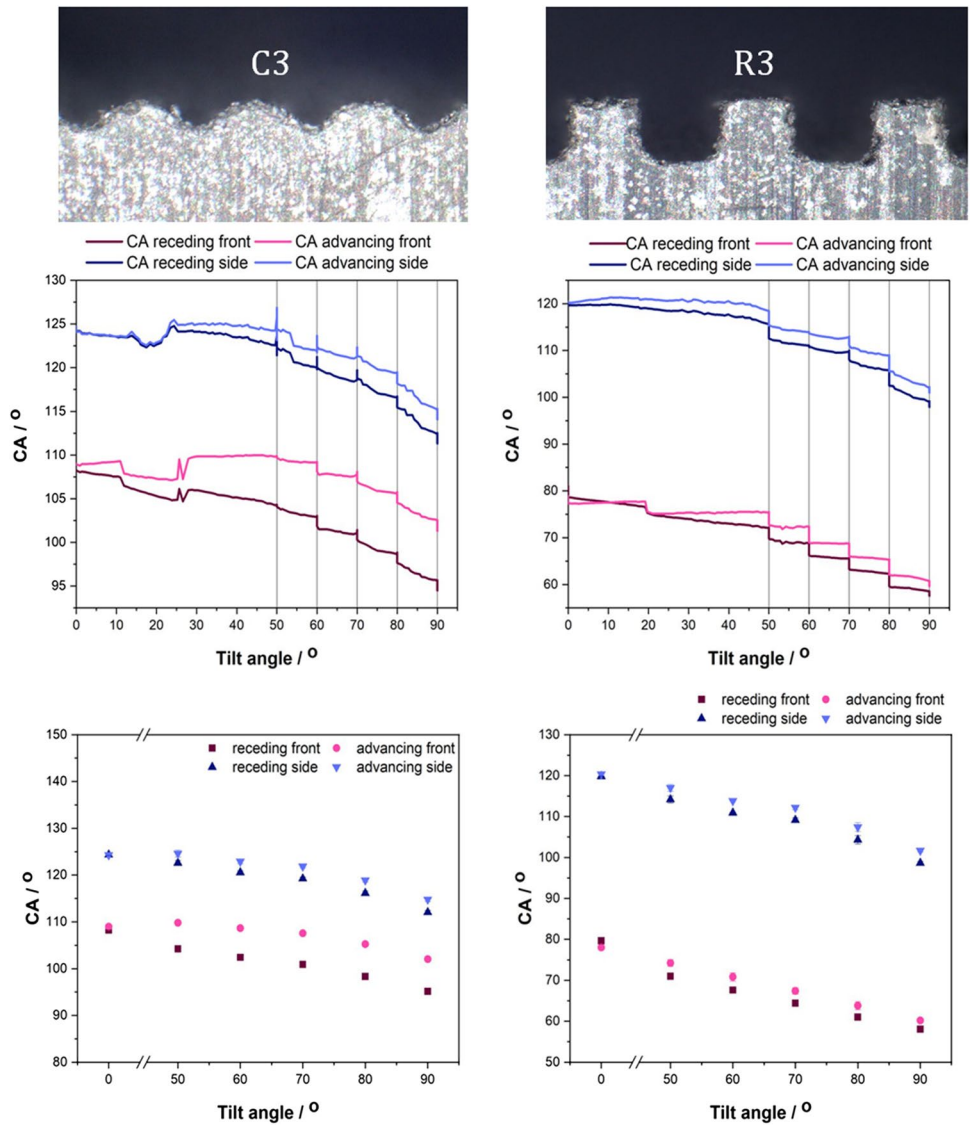

Fig. 11 Contact angle evolution with increasing tilting angle of platform for C3 and R3

was not reported. This result may be attributed to the fact that in the case of I2 type, the droplet was never completely soaked inside the cavity throughout the whole tilting process, whereas in the case of D5, the droplet was completely soaked in. When the droplet is soaked in the cavities, the side movement is highly restricted.

3.4 The effect of drop volume, different wetting liquids, and time-dependent wettability durability on different profile types

In this section, the fluctuation of SCA on various profile types is reported when different droplet volumes were used. SCA was measured also for acetone and ethylene glycol, two liquids with lower surface tension than water. Moreover, the SCA of selected samples was measured after 3 months in order to examine their wettability durability over time.

Figure 14 shows the average for each group type measurements of the SCA for 2 μl and 5 μl. It can be observed that for all profile group types, the increase of the volume of droplet results in the rise of the SCA independently of the geometry type. From the results of Fig. 14, it can be observed that regarding low droplet volumes, the hierarchical effect of the increase of wettability reported previously which was induced by dual-scale roughness does not apply. In almost all types considered, the average SCA is extremely close with the SCA of the flat-machined surface. Thus, the effect of the second scale of roughness demonstrated a lower limit of activation strongly related to the smaller dimension scale of features designed in this work. In the case of the D group, the SCA of the 2-μl volume droplet had a great difference compared to the other types, showing clear hydrophilicity. It seems that the double geometry types induce the opposite effect of hierarchy for low droplet volumes,

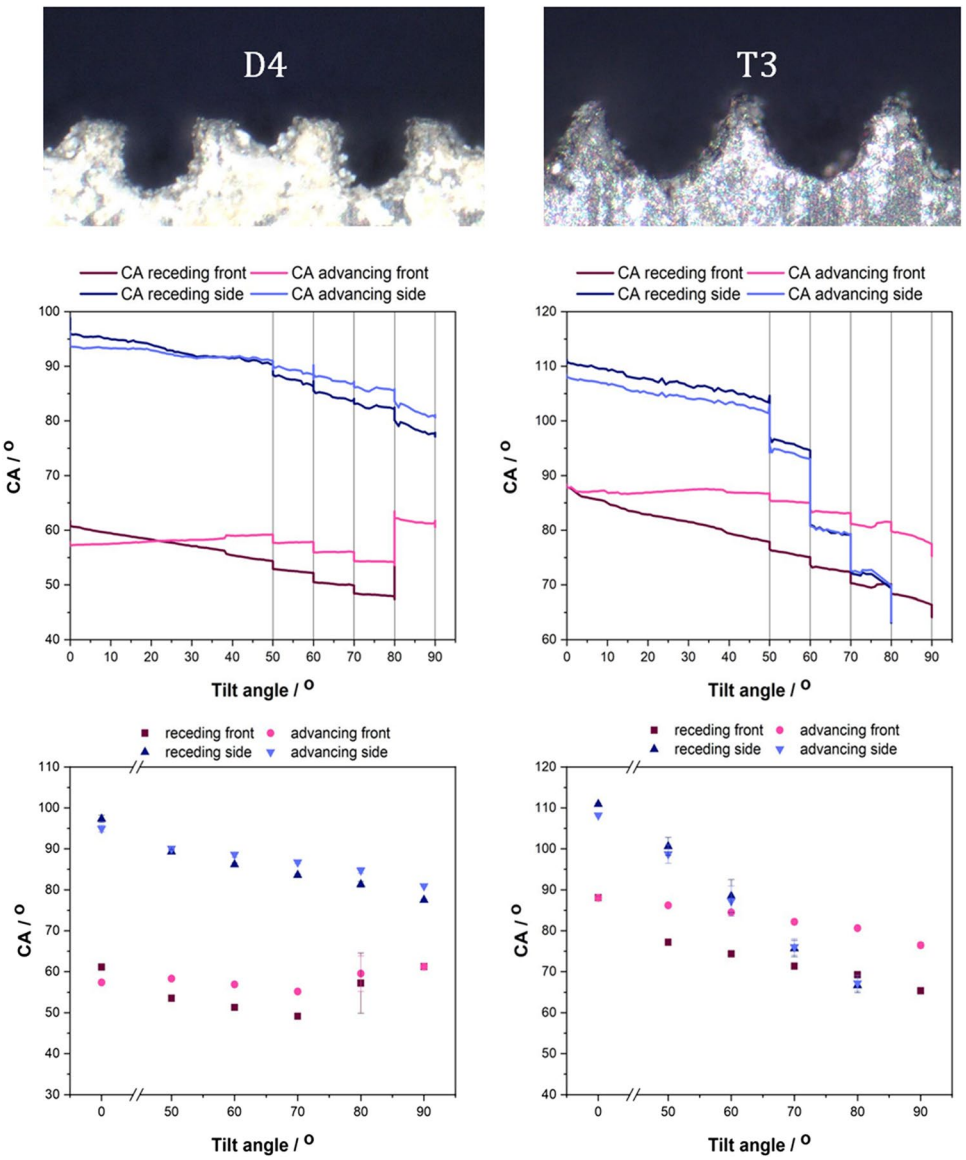

Fig. 12 Contact angle evolution with increasing tilting angle of platform for D4 and T3

possibly due to their combined structure. The higher volume grooves are facilitating the droplet's initial soaking and the adjacent lower volume grooves serve as extra reservoirs for the rest of the droplet volume. This combination allows the majority of the volume of the droplet to be soaked inside the cavities, resulting in lower SCA. For a droplet with higher volume, the majority of its volume will be above the surface, increasing its SCA.

After these observations, the effect of droplet volume in SCA was also tested in particular profile types concerning their feature dimensions or geometrical complexity as well as higher droplet volume, as seen in Fig. 15. For that cause, three rectangular type profiles with increasing groove width and height (R1, R2, and R4) were chosen. Regarding geometrical complexity, a case of double-sized grooves (D3) and two cases of re-entrant profiles (I1 and I2) were selected. The three R type geometries retained the double-scale improvement in SCA for all droplet volumes tested. As the relative dimension of the droplet radius with the groove width increased, no decreasing trend was observed, opposing to relevant study [36]. However, it was confirmed that with higher droplet volumes, the SCA was decreased in all cases considered. As mentioned before, the D4 geometry demonstrates hydrophilicity at low droplet volumes, although at middle and higher volumes, it becomes hydrophobic. Again, higher droplet volume causes a decrease in SCA. Even at middle droplet volume, this profile type was reported to be hydrophilic [24]. The two re-entrant geometries showed a similar trend, having the best hydrophobic performance at 5 μl. It is worth mentioning that the I type grooves did not get wet in any case considered, effectively trapping air inside the cavities [27]. The I2 type showed fewer fluctuations in

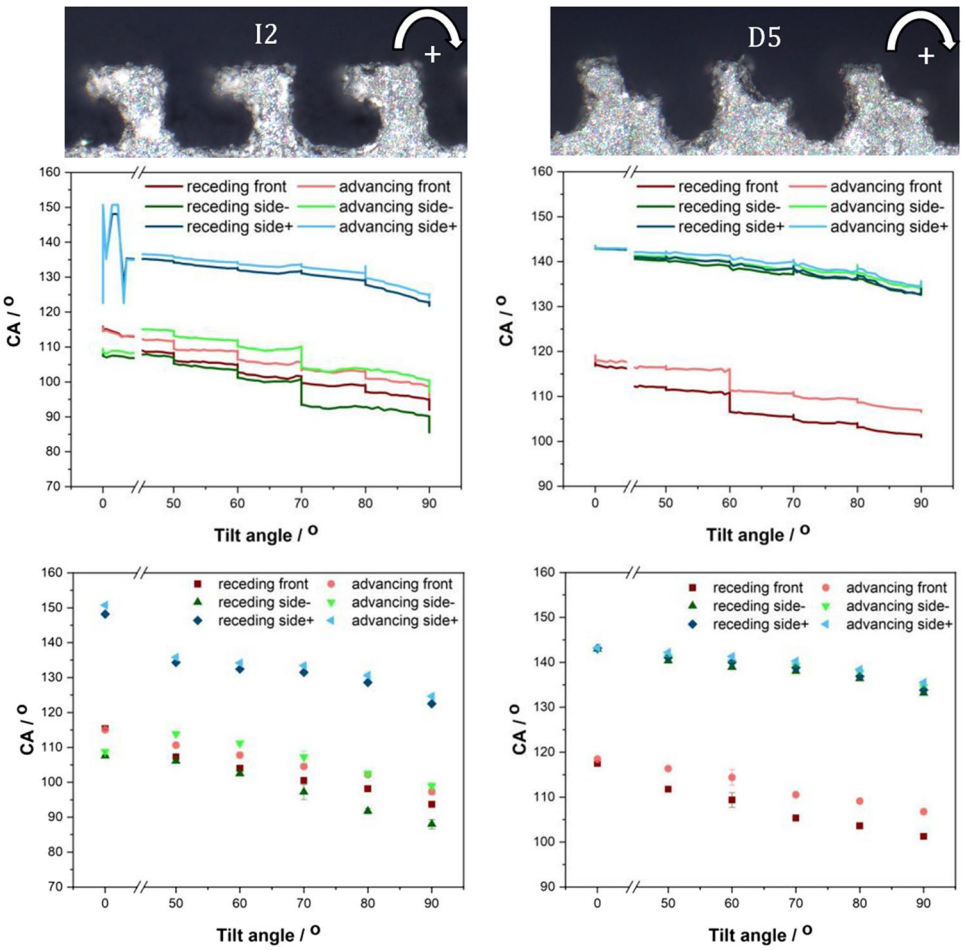

Fig. 13 Contact angle evolution with increasing tilting angle of platform for D4 and T3

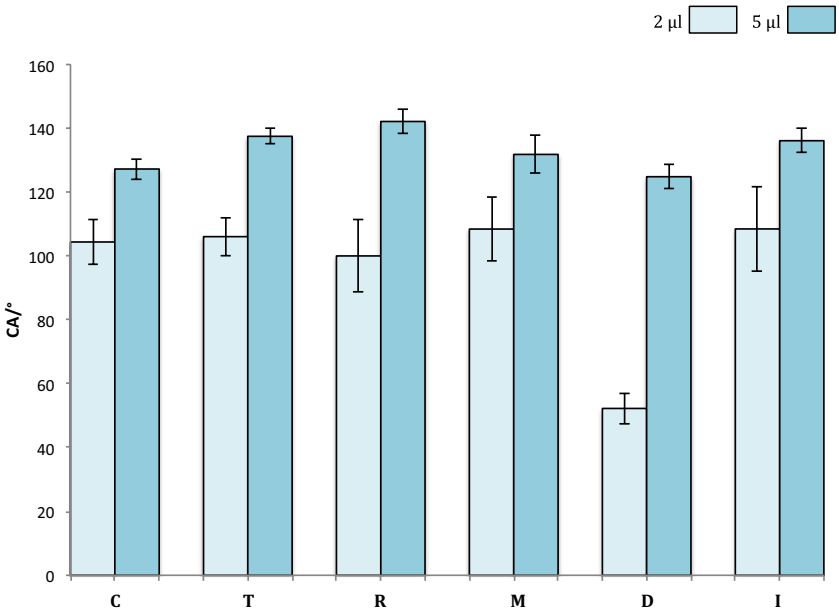

Fig. 14 Average contact angle for each profile group for droplet volumes of 2 µl and 5 µl

SCA for all three different droplet volumes tested between the measured samples. The I2 type showed significant lower SCA with both low and high droplet volumes. This difference can be attributed to the fact that it has smaller feature lengths than I1, despite the fact that the upper groove width is almost the same for both types. Consequently, more

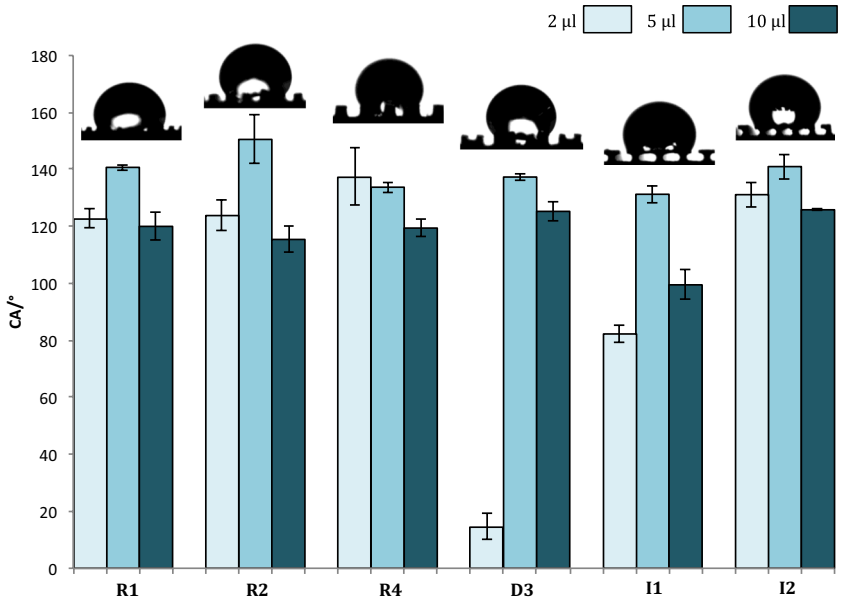

Fig. 15 Contact angle of selected profile types for droplet volumes of 2 µl, 5 µl, and 10 µl. Droplets of 10 µl volume are depicted in the images above columns

pockets can support the droplet even at lower droplet volumes. This mechanism does not apply to fully wetted surfaces such as R type, as can be seen from Fig. 15.

Dual-scale structures prepared via WEDM process are reported on some occasions to be amphiphobic with lower surface tension liquids than water, such as ethylene glycol [28, 60] and peanut oil [61]. However, in these works, an extra surface coating process step was included in order to modify the surface chemistry towards amphiphobicity. In the present work, no extra step of chemical modification was utilized. Consequently, the SCA of the low surface tension liquids that were tested, namely, acetone (25.2 mN/m) and ethylene glycol (48.2 mN/m), was well below 10°, exhibiting superliquiphilicity.

An interesting feature of preparation of dual-scale surface structures via WEDM process is their time-dependent wettability. It is reported that for various types of aluminum profiles, the hydrophobic property is attained at least after 2–3 days of exposure to the atmosphere [34]. This feature was confirmed also by this study. In order to investigate the effect of much longer periods of exposure in the atmosphere, SCA measurements were performed on selected samples from front and side direction after the pass of 3 months. The results are depicted in Fig. 16. The samples were not cleaned before the wettability tests after 3 months, so that the effect of exposure is clear.

For the simple geometrical profiles R4 and T3, it can be seen that the effect of time decreased the degree of hydrophobicity in both side and front directions. However, the surfaces remained hydrophobic. Hierarchical surfaces of aluminum alloys have been reported to increase their hydrophobicity until a 30-day period of exposure in ambient air [62, 63]. In this work, it is reported that after a much longer period, the degree of hydrophobicity is decreased. This can be attributed to the adsorption of atmospheric elements that can alter the chemistry and subsequently the wettability of the surface. A different trend was observed from the I1 profile type. This deviation is most likely attributed to the different wetting mechanisms of the re-entrant geometries that were described in the previous sections, in which air entrapment at the mesoscale and not surface chemistry or microroughness acts as the dominant cause of the hydrophobic property.

3.5 Applications related to dual-scale hydrophobic surfaces prepared by WEDM

As elucidated in the introduction, superhydrophobicity can lead to surface functionalization towards obtaining several surface attributes, such as anti-fouling, anti-icing, or drag reduction. Regarding the category of superhydrophobic metallic materials and more specifically aluminum alloys, surface functionalization stemming from dual-scale structures can play an important role in several applications of various industrial sectors.

Aluminum alloys are commonly used on high stress structural applications or as components for parts of the automotive sector, where corrosion resistance is of great importance [64]. WEDM texturing has been experimentally proven to improve corrosion resistance of metals, by inducing roughness and reducing wettability of the surface [65]. In addition, hierarchical structures can provide effective anti-fouling attributes. In marine applications, many metallic structural ship components are facing unwanted fouling, yielding higher fuel costs due to speed loss [66]. Structured surfaces prepared by EDM can exhibit

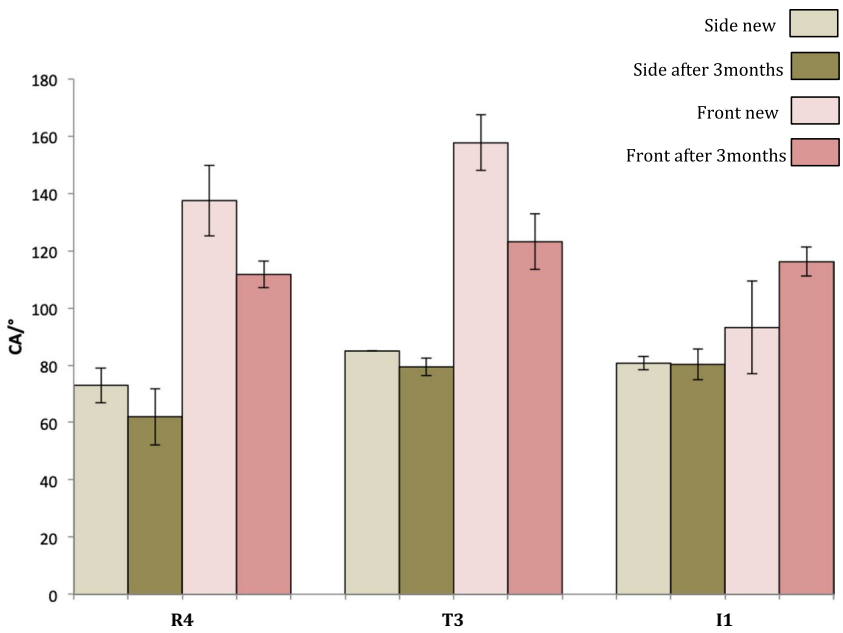

Fig. 16 Contact angles from side and front between the lapses of 3 months

promising anti-fouling properties inhibiting fouling adhesion [67]. Additionally, anti-biofouling properties reported by metallic parts fabricated by WEDM [33] pose discharge machining as promising process for the biomedical sector. Regarding aerospace industry, where aluminum alloys are also common utilized materials, surface attributes such as anti-icing or drag reduction can be cost saving [68]. Anti-icing property can be realized via the WEDM process by creating less adhesion with the freezing droplet [69], while directionality induced by mesoscale grooves can lead to improved drag reduction derived from the sharkskin effect. Finally, the property of combined hydrophobicity and superoleophilicity of a grooved surface, such as the surface structures fabricated in the present work, constitutes an ideal candidate for oil/water separation applications [26].

While dual-scale hydrophobic structures can be fabricated by various methods, such as laser texturing or chemical methods, the WEDM offers a one-step facile process for the cost-effective and chemical-free realization of superhydrophobic metallic surfaces. It can be deducted that via the WEDM process, structures with attributes much wanted on various industrial applications can be realized, as schematically depicted in Fig. 17. In this work, the rise of superhydrophobicity was made possible by appropriate tuning of roughness parameter values of the mesoscale superimposed with quite high initial wettability values of the smaller scale microroughness. Selecting an optimized machining parameter combination can further increase the hydrophobicity of the smaller scale, leading to a further overall increase of the hydrophobicity of the dual-scale structure. Future works are highly encouraged to be carried out regarding the testing of the before-mentioned surface attributes of metallic surfaces produced by WEDM process in an industrial scale.

4 Conclusion

In this work, the WEDM process was utilized for the one-step preparation of dual-scale aluminum alloy samples. The smaller scale microroughness was created via the material removal from discharging while the larger scales grooves were realized through the CNC wire path. This dual-scale morphology delivered a great rise in the hydrophobicity of all the surfaces. The effects of various groove profile geometry types along with their roughness parameters were investigated in terms of static hydrophobicity. Moreover, the effect that anisotropy of selected geometry types had on dynamic conditions of surface tilting up to 90° was examined. Finally, the effects of different drop volumes and lower surface tension liquids as well as the durability of the hydrophobicity of the samples after the lapse of 3 months were considered through changes in SCA measurements. The most important results were found to be as follows:

1. The average rise of SCA compared with the flat WEDMed surface, considering all the samples, was found at 30°. Between different profile geometry groups, the most hydrophobic was the R type, while the most hydrophobic sample was the T3.
2. A strong correlation ($R > 90\%$) of roughness parameters Ra, Rz, and Rp and SCA was found for the groove profiles with simple geometry (C, T, R), showing a wettability minimum for Ra = 70 μm, Rz = 240 μm, and Rp = 160

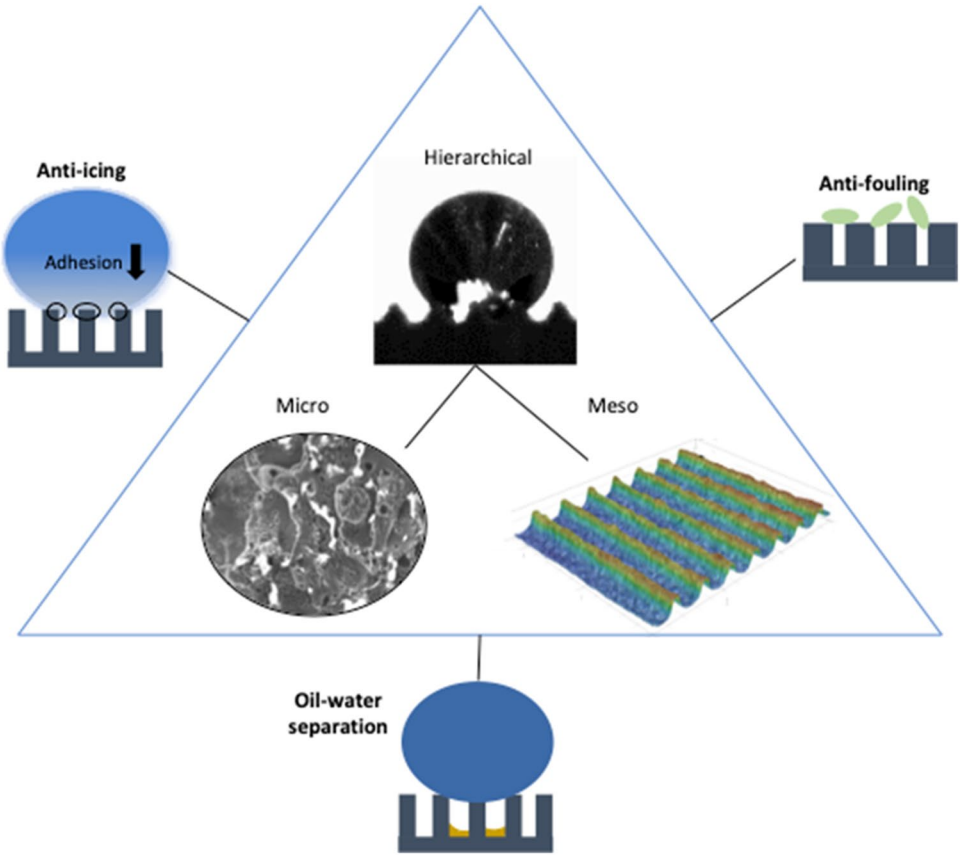

Fig. 17 Application instances for dual-scale surfaces fabricated via WEDM

μm. In addition, concerning all geometry types, negative Rsk (< -1.3) or too high Rku (> 1.6) had a negative effect on hydrophobicity, while near-zero or positive Rsk was found in the most hydrophobic samples. These results may encourage the use of roughness parameters as design principles for the manufacturing of the larger scale of dual-scale surfaces.

3. All samples that were tested for tilting exhibited strong droplet adhesion in all directions. Concerning front and side directions, the T3 type was more affected by surface tilting, degrading its anti-wetting property. On the contrary, D4 retained better its hydrophobic properties, due to its double-sized grooves. Concerning (+) and (−-) side directions, D5 was able to retain its hydrophobic properties in both directions, while I2 facilitated spreading through the (−) side direction of its features.
4. Almost all the samples exhibited their highest SCA at medium droplet volumes (5 μl). For low droplet volumes (2 μl), the effect of scale duality is not significantly affecting wettability. At low droplet volumes, the D profile type was hydrophilic, due the total larger groove volume. The two re-entrant types I effectively trapped air inside their cavities, for all droplet volumes tested. It was found that the more segmented the cavity volume is, the more hydrophobic the surface becomes, considering all droplet volumes.
5. All samples were superliquiphilic for lower surface tension liquids, ethanol glycol, and acetone.
6. After 3 months, the tested samples retained a reduced hydrophobicity compared to the initial except I1, probably due to different wetting mechanisms.

Funding Open access funding provided by HEAL-Link Greece. This work was co-financed by Greece and the European Union (European Social Fund-ESF) through the Operational Programme "Human Resources Development, Education and Lifelong Learning" in the context of the Act "Enhancing Human Resources Research Potential by undertaking a Doctoral Research" Sub-action 2: IKY Scholarship Programme for PhD candidates in the Greek universities.

Declarations

Competing interests The authors declare no competing interests.

References

1. Xia D, Johnson LM, López GP (2012) Anisotropic wetting surfaces with one-dimesional and directional structures: fabrication approaches, wetting properties and potential applications. Adv Mater 24:1287–1302
2. Kim W, Kim D, Park S, Lee D, Hyun H, Kim J (2018) Engineering lotus leaf-inspired micro-and nanostructures for the manipulation of functional engineering platforms. J Ind Eng Chem 61:39–52
3. Nishimoto S, Bhushan B (2013) Bioinspired self-cleaning surfaces with superhydrophobicity, superoleophobicity, and superhydrophilicity. RSC Adv 3:671–690
4. Patankar NA (2004) Mimicking the lotus effect: influence of double roughness structures and slender pillars. Langmuir 20:8209–8213
5. Alvarez K, Hyun S-K, Fujimoto S, Nakajima H (2008) In vitro corrosion resistance of Lotus-type porous Ni-free stainless steels. J Mater Sci - Mater Med 19:3385–3397
6. Bixler GD, Bhushan B (2013) Fluid drag reduction and efficient self-cleaning with rice leaf and butterfly wing bioinspired surfaces. Nanoscale 5:7685–7710
7. Wenzel RN (1936) Resistance of solid surfaces to wetting by water. Ind Eng Chem 28:988–994
8. Cassie ABD, Baxter S (1944) Wettability of porous surfaces. Trans Faraday Soc 40:546–551
9. Nosonovsky M, Bhushan B (2008) Multiscale dissipative mechanisms and hierarchical surfaces: friction, superhydrophobicity, and biomimetics. Springer Science & Business Media. https://doi.org/10.1007/978-3-540-78425-8
10. Guo P, Lu Y, Ehmann KF, Cao J (2014) Generation of hierarchical micro-structures for anisotropic wetting by elliptical vibration cutting. CIRP Ann 63:553–556
11. Zhu J, Hu X (2019) A new route for fabrication of the corrosion-resistant superhydrophobic surface by milling process. J Coat Technol Res 16:249–255
12. Prasad KK, Roy T, Goud MM, Karar V, Mishra V (2020) Diamond turned hierarchically textured surface for inducing water repellency: analytical model and experimental investigations. Int J Mech Sci 193:106140
13. Peng Q, Jia L, Ding Y, Dang C, Yin L, Yan X (2020) Influence of groove orientation on dropwise condensation on hydrophobic and hierarchical superhydrophobic surfaces with microgroove arrays. Int Commun Heat Mass Transfer 112:104492
14. Yuan Y, Zhang D, Jing X, Zhu H, Zhu W-L, Cao J et al (2019) Fabrication of hierarchical freeform surfaces by 2D compliant vibration-assisted cutting. Int J Mech Sci 152:454–464
15. Fu Y, Zhao Z, Yip W, To S (2020) Novel fabrication of a hierarchical structured surface with improved corrosion inhibition by using hydrothermal synthesis and ultraprecision machining. Surf Coat Technol 385:125432
16. Anagnostopoulos A, Nikulin A, Knauer S, Bondarchuk O, Rivero MEN, Lu T et al (2023) Fabrication of superhydrophobic metallic porous surfaces via CO2 and water processing. Appl Surf Sci 632:157546
17. Gao M, Wang DP, Huang YF, Meng S, Wang WH (2016) Tunable hydrophobicity on fractal and micro-nanoscale hierarchical fracture surface of metallic glasses. Mater Des 95:612–617
18. Rukosuyev MV, Lee J, Cho SJ, Lim G, Jun MBG (2014) One-step fabrication of superhydrophobic hierarchical structures by femtosecond laser ablation. Appl Surf Sci 313:411–417
19. Martínez-Calderon M, Rodríguez A, Dias-Ponte A, Morant-Miñana MC, Gómez-Aranzadi M, Olaizola SM (2016) Femtosecond laser fabrication of highly hydrophobic stainless steel surface with hierarchical structures fabricated by combining ordered microstructures and LIPSS. Appl Surf Sci 374:81–89
20. Xing W, Li Z, Yang H, Li X, Wang X, Li N (2019) Anti-icing aluminum alloy surface with multi-level micro-nano textures constructed by picosecond laser. Mater Des 183:108156
21. Su Y, Zhao Y, Jiang S, Hou X, Hong M (2021) Anisotropic superhydrophobic properties of bioinspired surfaces by laser ablation of metal substrate inside water. Adv Mater Interfaces 8:2100555
22. Bae WG, Song KY, Rahmawan Y, Chu CN, Kim D, Chung DK et al (2012) One-step process for superhydrophobic metallic surfaces by wire electrical discharge machining. ACS Appl Mater Interfaces 4:3685–3691
23. Chen Z, Yan Z, Zhou H, Han F, Zhao L, Yan H (2021) One-step fabrication of the wear-resistant superhydrophobic structure on SiCp/Al composite surface by WEDM. Surf Coat Technol 409:126876
24. Ouyang L, Liu J, Xiao Y, Zhang Y, Xie G, Zhang H et al (2022) One-step preparation of a superhydrophobic surface by electric discharge machining with a carbon fiber brush electrode. Langmuir 38:9853–9862
25. Wan Y, Lian Z, Xu J, Weng Z, Yin X, Yu H (2014) Fabrication of the stainless steel surface with super durable one-direction superhydrophobicity and two-direction anisotropic wettability. Micro & Nano Letters 9:712–716
26. Bae W-G, Kim D, Song KY, Jeong HE, Chu CN (2015) Engineering stainless steel surface via wire electrical discharge machining for controlling the wettability. Surf Coat Technol 275:316–323
27. Weisensee PB, Torrealba EJ, Raleigh M, Jacobi AM, King WP (2014) Hydrophobic and oleophobic re-entrant steel microstructures fabricated using micro electrical discharge machining. J Micromech Microeng 24:095020
28. Yu H, Lian Z, Wan Y, Weng Z, Xu J, Yu Z (2015) Fabrication of durable superamphiphobic aluminum alloy surfaces with anisotropic sliding by HS-WEDM and solution immersion processes. Surf Coat Technol 275:112–119
29. Liang Y, Peng J, Li X, Huang J, Qiu R, Zhang Z et al (2017) Wettability and contact time on a biomimetic superhydrophobic surface. Materials 10:254
30. Chu X, Zeng X, Zhuang W, Zhou W, Quan X, Fu T (2019) Vibration assisted high-speed wire electric discharge machining for machining surface microgrooves. J Manuf Process 44:418–426
31. Chen S, Wang R, Wu F, Zhang H, Gao X, Jiang L (2021) Copper-based high-efficiency condensation heat transfer interface consisting of superhydrophobic hierarchical microgroove and nanocone structure. Mater Today Phys 19:100407
32. Wu C, Wu X, Zhao H, Xu B, Zhu L, Liu Y et al (2020) Effect of sub-millimetre morphologies on the hydrophobicity of a copper surface prepared by WEDM. Surf Coat Technol 385:125455
33. Prakash V, Priyadarshni N, Das AK, Chattopadhyay S (2022) Fabrication of hydrophobic surface on Ti6Al4V by WEDM process for surgical instruments and bioimplants. Int J Adv Manuf Technol 118:111–1123

34. Xiao Y, Zhang Y, Yan Y, Guo Z, Liu J, Can W (2021) Study of wettability transition on hierarchical structured aluminum cut by wire electric discharge machining. Colloids Surf, A 627:127200
35. Zhang Y, Yang X, Wang S, Liu J, Liu X, Chan K et al (2023) Multifunctional superhydrophobic copper mesh for efficient oil/water separation and fog collection. Colloids Surf, A 657:130603
36. Du H, Zhao S, Ma Z, Liu J, Xiao G, Li W et al (2022) The size effect on contact angles and dynamic behaviors of droplets on microcolumn and microstrip array surfaces. Adv Eng Mater 24:2101568
37. Dong J, Jin Y, Dong H, Liu J, Ye S (2018) Numerical study for a large-volume droplet on the dual-rough surface: apparent contact angle, contact angle hysteresis, and transition barrier. Langmuir 34:8119–8127
38. Wang H, Chi G, Li L, Gong S, Zhu J, Tian C et al (2021) Numerical calculation of apparent contact angles on the hierarchical surface with array microstructures by wire electrical discharge machining. Langmuir 37:1768–1778
39. Li Z, Liu Y, Li W, Cao B, Dai Y (2022) Modeling of two-scale array microstructure and prediction of apparent contact angle based on WEDM. Int J Adv Manuf Technol 121:2699–2719
40. Baffari D, Buffa G, Campanella D, Valvo EL, Fratini L (2018) Experimental and numerical investigation on a new FSW based metal to composite joining technique. J Manuf Process 34:758–764
41. Barati M, Abbasi M, Abedini M (2019) The effects of friction stir processing and friction stir vibration processing on mechanical, wear and corrosion characteristics of Al6061/SiO2 surface composite. J Manuf Process 45:491–497
42. Chowdhury SG, Mondal A, Gubicza J, Krállics G, Fodor A (2008) Evolution of microstructure and texture in an ultrafine-grained Al6082 alloy during severe plastic deformation. Mater Sci Eng, A 490:335–342
43. Zhang L, Wu H, Wen J, Li M, Shao X, Ma X (2022) Glass to aluminum joining by forming a mechanical pin structure using femtosecond laser. J Mater Process Technol 302:117504
44. Moroni G, Syam WP, Petrò S (2018) A simulation method to estimate task-specific uncertainty in 3D microscopy. Measurement 122:402–416
45. Leksycki K, Królczyk JB (2021) Comparative assessment of the surface topography for different optical profilometry techniques after dry turning of Ti6Al4V titanium alloy. Measurement 169:108378
46. Podulka P, Macek W, Zima B, Lesiuk G, Branco R, Królczyk G (2023) Roughness evaluation of turned composite surfaces by analysis of the shape of autocorrelation function. Measurement 222:113640
47. Feng CC, Li L, Zhang CS, Zheng GM, Bai X, Niu ZW (2019) Surface characteristics and hydrophobicity of Ni-Ti alloy through magnetic mixed electrical discharge machining. Materials 12:388
48. Peta K, Bartkowiak T, Galek P, Mendak M (2021) Contact angle analysis of surface topographies created by electric discharge machining. Tribol Int 163:107139
49. Guo C, Koshy P, Coelho F, Selvaganapathy PR (2019) Sink electrical discharge machining of hydrophobic surfaces. CIRP Ann 68:185–188
50. Kietzig A-M, Hatzikiriakos SG, Englezos P (2009) Patterned superhydrophobic metallic surfaces. Langmuir 25:4821–4827
51. Long J, Zhong M, Zhang H, Fan P (2015) Superhydrophilicity to superhydrophobicity transition of picosecond laser microstructured aluminum in ambient air. J Colloid Interface Sci 441:1–9
52. Li X-M, Reinhoudt D, Crego-Calama M (2007) What do we need for a superhydrophobic surface? A review on the recent progress in the preparation of superhydrophobic surfaces. Chem Soc Rev 36:1350–1368
53. Chen L, Guo Z, Liu W (2017) Outmatching superhydrophobicity: bio-inspired re-entrant curvature for mighty superamphiphobicity in air. J Mater Chem A 5:14480–14507
54. Kim J, Sim SO, Park HW (2016) Fabrication of durable hydrophobic micropatterns on stainless steel using a hybrid irradiation process. Surf Coat Technol 302:535–542
55. Chen Z, Wu C, Zhou H, Zhang G, Yan H (2022) A high-efficiency preparation method of super wear-resistant superhydrophobic surface with hierarchical structure using wire electrical discharge machining. Surf Coat Technol 444:128673
56. Boscher ND, Vaché V, Carminati P, Grysan P, Choquet P (2014) A simple and scalable approach towards the preparation of superhydrophobic surfaces–importance of the surface roughness skewness. J Mater Chem A 2:5744–5750
57. Tang X, Tian Y, Tian X, Li W, Han X, Kong T et al (2021) Design of multi-scale textured surfaces for unconventional liquid harnessing. Mater Today 43:62–83
58. Cai Z, Chen F, Tian Y, Zhang D, Lian Z, Cao M (2022) Programmable droplet transport on multi-bioinspired slippery surface with tridirectionally anisotropic wettability. Chem Eng J 449:137831
59. Nakajima D, Kikuchi T, Natsui S, Suzuki RO (2018) Advancing and receding contact angle investigations for highly sticky and slippery aluminum surfaces fabricated from nanostructured anodic oxide. RSC Adv 8:37315–37323
60. Lian Z, Wan Y, Xu J, Yu H, Weng Z (2015) HS-WEDM machining of superamphiphobic al surfaces and effect of the droplet size on wettability. In: 2015 International Conference on Manipulation, Manufacturing and Measurement on the Nanoscale (3M-NANO). IEEE, pp 22–26
61. Lian Z, Xu J, Wang Z, Weng Z, Wan Y, Zhang L et al (2016) Research on HS-WEDM and chemical etching technology of superamphiphobic surfaces on Al substrates. Micro Nano Lett 11:425–429
62. Shirsath GB, Muralidhar K, Pala RGS, Ramkumar J (2019) Condensation of water vapor underneath an inclined hydrophobic textured surface machined by laser and electric discharge. Appl Surf Sci 484:999–1009
63. Yang Z, Liu X, Tian Y (2019) Insights into the wettability transition of nanosecond laser ablated surface under ambient air exposure. J Colloid Interface Sci 533:268–277
64. Liu M, Guo Y, Wang J, Yergin M (2018) Corrosion avoidance in lightweight materials for automotive applications. NPJ Mater Degrad 2:24
65. Li X, Shi T, Li B, Chen X, Zhang C, Guo Z et al (2019) Subtractive manufacturing of stable hierarchical micro-nano structures on AA5052 sheet with enhanced water repellence and durable corrosion resistance. Mater Des 183:108152
66. Magin CM, Cooper SP, Brennan AB (2010) Non-toxic antifouling strategies. Mater today 13:36–44
67. He ZR, Luo ST, Liu CS, Jie XH, Lian WQ (2019) Hierarchical micro/nano structure surface fabricated by electrical discharge machining for anti-fouling application. J Market Res 8:3878–3890
68. Antonini C, Innocenti M, Horn T, Marengo M, Amirfazli A (2011) Understanding the effect of superhydrophobic coatings on energy reduction in anti-icing systems. Cold Reg Sci Technol 67:58–67
69. Qiu R, Li Z, Wu Z (2019) Enhanced anti-icing and anti-corrosion properties of wear-resistant superhydrophobic surfaces based on Al alloys. Mater Res Express 6:045059